"Neuronal Oscillations on Evolving Networks: Dynamics, Damage, Degradation, Decline, Dementia and Death": A review and extension of Goreily et al. (2020)

Shayan Shafquat,[1] Zongyuan Cai,[1] Youssef Hafid,[1] and Zakaria Taghi[1]
[1]*School of Psychology, University of Nottingham, Nottingham, NG7 2RD, UK*
(Dated: May 6, 2024)

The paper "Neuronal Oscillations on Evolving Networks: Dynamics, Damage, Degradation, Decline, Dementia, and Death" by Goreily et al. (2020) delves into the effects of neurodegenerative diseases on brain neural networks [1]. The degradation caused by these diseases affects not only the nodes themselves but the strength of the connections between these nodes. The resulting connectome evolves as the disease progresses, with damage caused by the disease affecting the spreading of the disease, although minutely. The progression of the disease is modelled through both toxic protein accumulation and rest-state activity. In this paper, we attempt to recreate the results of their study and delve further into extending their work and understanding the implications of their model. Protein seed concentration and the diffusion model used both influence the damage accumulation in the connectome. This is reflected in the decay in both neural activity within the neural mass model as well as a decay in axonal velocity. Our findings reinstate that changes in edge weights have a limited impact on the disease's progression. However, dynamic biomarkers have been effective in forecasting a significant cognitive decline over a decade.

I. INTRODUCTION

A. Biology

Alzheimer's disease (AD) is a progressive neurodegenerative disorder leading to severe cognitive and functional impairments. These symptoms are a result of synaptic dysfunction and death of neurons, particularly in the hippocampus and other parts of the cerebral cortex[2]. The major hallmarks of AD include the pathological deposition of amyloid-beta (Aβ) plaques and neurofibrillary tangles composed of tau protein in the brain, both contributing to neuronal loss and brain atrophy[3]

The onset of AD is typically in later life, however there is evidence suggesting that prior to noticeable symptoms, there are measureable changes to neural biomarkers. Given evidence that that early intervention results in improved patient outcomes[4], developing a reliable early indicator or AD is of huge clinical importance.

B. Modelling

We replicate the model of Goriely et al[1], combining a long term protein spread model following a prion-like paradigm with a neural biomarker model, prompted by evidence linking degenerative diseases to misfolded proteins[2], [3], [5]. Basing their initial conditions and connections on the Budapest Reference Connectome v3.04,[6] they modelled disease progression as an evolving undirected graph, and toxic protein accumulation within nodes modelled using the Fisher-Kolmogorov-Petrovsky-Piskunov equation. Change in damage was quantified and modelled within individual nodes based on toxic protein toxicity, toxic protein concentration, and current node damage, modelling changes in connectivity based on node damage. The nodes selected for initial seeding with toxic protein were those representing the entorhinal area, based on research suggesting it may be the initial locus of neurofibrillary tangles caused by misfolded tau proteins withing Alzheimer's disease progression[7]. Using structural biomarkers they observed even unrealistically high damage made negligible difference to the rise in concentration over time. This modelled the behaviour of pathogenic protein seeding, by the time network damage hinders diffusion, the misfolded proteins have already infiltrated and begun self replication. They were also able to model disease staging through the brain by noting the variation in levels of damage between different regions over the time course of the disease. At each node, they used a Wilson-Cowan[8] type neural mass model to model brain activity, with nodes connected through a delay differential equation with parameters chosen to approximate those in Deco et al[9], due to their validation using resting state fMRI. Modelling neural activity at intervals throughout disease progression, and monitoring biomarkers associated with neurodegenerative disease in varying regions (the overall power in the Gamma range, the average oscillatory activity, and the metastability index). They were able to model the decline of biomarkers, linking the phenomenon to damage induced by toxic protein accumulation, as well as observe their changes over disease progression. Our aim is to replicate the model, as well as implement the more biologically accurate heterodimer model of protein conversion[10]. We also aim to utilize the model to investigate disease progression variation between hemispheres.

C. Aims

- To replicate the neural mass and the resting-state dynamics model and extend the findings of Goriely

et al. [1]

- To investigate how disease progression differs between hemispheres within the model
- To replicate the model of Fornari et al[10] which also implemented a heterodimer model of protein spread and compare it's results to that of Goriely et al's model.

II. METHODS

One key characteristic of prion-like diseases involves the propagation of misfolded proteins, which initially affect a localized area and subsequently extend along axonal pathways to pervade the entire brain [11]. This propagation process is conceptualized as diffusion through the brain's connectome, depicted as a weighted undirected graph, denoted by $\mathcal{G}_0$, consisting of N nodes and E edges.

A. The connectivity-weighted graph

The initial connectome graph $\mathcal{G}_0$ is derived from diffusion tensor magnetic resonance imaging data collected from 418 healthy individuals participating in the Human Connectome Project. This extraction utilizes the Budapest Reference Connectome v. 3.0 framework [12]. For illustrative purposes, a high-resolution connectome with 1015 nodes and 37,477 edges is transformed into a more accessible representation with 83 nodes and 1,130 edges (figure 1.

The structure of the connectome, $\mathcal{G}_T$, reflects an undirected updating weighted graph, observable at any time $T \geq 0$, with $\mathcal{G}_0$ serving as the starting point. Each node k represents a specific brain region in R_s, where s ranges from 1 to 7, including the frontal, parietal, temporal, and occipital lobes, as well as the limbic system, the basal ganglia, and the brain stem.

Incorporating the methodology established by Goriely, Kuhl, and Bick [1], we first define the adjacency matrix W, which is a graph-based representation of the connectome ($\mathcal{G}_T$). The adjacency matrix is a numerical representation where each element w_{ij} denotes the weight of the connection between node i and node j as in Figure (1). These weights are calculated as $w_{ij} = n_{ij}/l_{ij}$, with n_{ij} indicating the number of axonal fibres connecting the nodes—reflecting potential pathways for neural communication—and l_{ij} representing the physical distance between these nodes, which influences signal transmission efficacy.

B. Graph Laplacian

This structured representation of brain connectivity is fundamental in constructing the Graph Laplacian L,

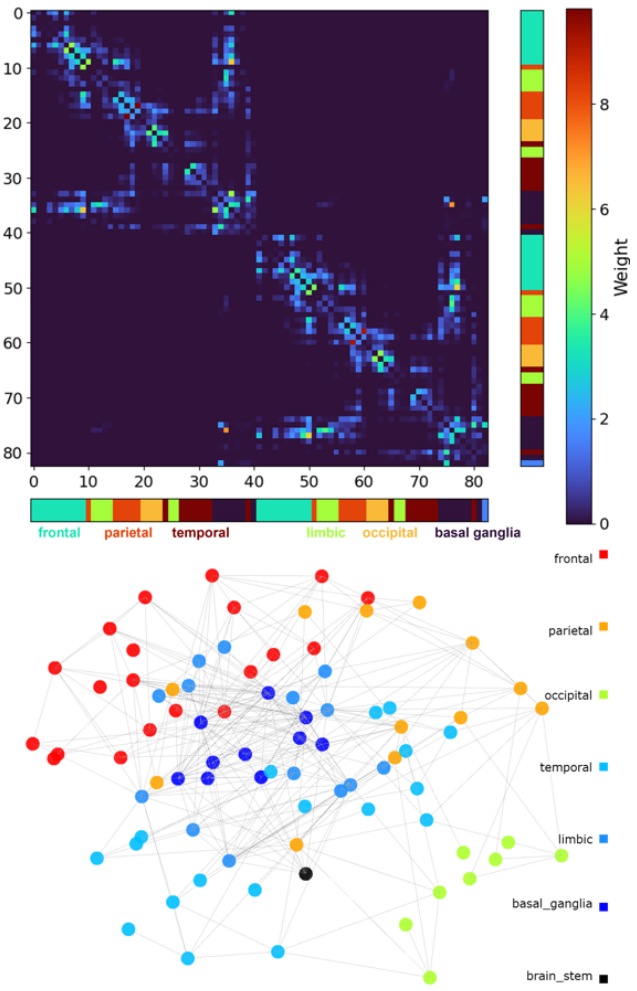

FIG. 1: The weighted connections in an 83-point connectome network indicate the density of fibres relative to the distances between nodes, with values ranging from 0 (blue) to 9.8 (red). The representation of different regions of interest as colour-coded nodes connected by edges is also included.

formulated as $L = \rho(D - W)$. Here, D is a diagonal matrix with entries $d_{kk} = \sum_{j=1}^{N} w_{kj}$, each summing the connection strengths w_{kj} for node k across the network. The factor ρ acts as a scalar adjusting the overall rate of transport across the network, modifying how influences propagate throughout the brain's network structure.

The Graph Laplacian L itself is instrumental in analyzing the network's dynamics. It allows for the exploration of how disturbances spread and how the brain maintains stability amidst these changes. It captures not just the local connectivity by reflecting the connection discrepancies at each node but also influences global network properties by describing overall connectivity and network responses to changes. Such analysis is crucial for understanding both normal brain functions and the impacts of neurodegenerative diseases.

C. Disease Progression

Goriely et al.'s [1] model quantified transport dynamics along the graph edges as a ballistic movement, temporally scaled using the velocity constant, ρ. This follows the prion-like paradigm, proposing nonlinear propagation of self-replicating toxic protein, and chosen due to previous success in using prion-like models to predict Alzheimer's disease volumetrics from MRI scans [13], and previous work where they were able to predict tau inclusions and amyloid deposits [14]. A representation of the brain connectome with 83 nodes, complemented by an adjacency matrix, is illustrated in (figure 1).

D. Protein Spread

1. *Fisher-Kolmogorov-Petrovsky-Piskunov*

We reproduced the spread of protein misfolding according to the Fisher-Kolmogorov-Petrovsky-Piskunov equation, selected by Goriely et al.[1] due to its ease of computation and prior performance emulating clinically observed Alzheimer's disease (AD) progression.

$$\dot{c}_k = -\sum_{j=1}^{N} L_{kj} c_j + \alpha c_k (1 - c_k), \quad k = 1, \ldots, N \tag{1}$$

2. *Heterodimer Model*

The Heterodimer model is the simplest kinetic model that accounts for the two possible configurations of the protein [15].

$$\rho = 0.01 mm/years$$

$$p + \tilde{p} \xrightarrow{k'_{11}} p\tilde{p} \quad p\,\tilde{p} \xrightarrow{k'_{12'}} \tilde{p}\tilde{p} \xrightarrow{k'_{22}} \tilde{p} + \tilde{p}. \tag{2}$$

Through this model, we can describe the transition from healthy proteins(p) to bonded proteins($p\widetilde{p}$) to polymer fragments($\tilde{p}$) as shown in equation (2). The misfolded protein binds to healthy proteins at rate $k_{11'}$. The bonded healthy protein is converted to an unhealthy protein at rate $k_{12'}$, and the bonded proteins fragment and become two separate misfolded protein fragments at a rate of $k_{1'2'}$ [10].

$$p + \tilde{p} \xrightarrow{k_{12}} \tilde{p} + \tilde{p}. \tag{3}$$

This equation can be simplified to represent the transition of one healthy and one misfolded protein into two misfolded proteins (See Equation 3). Using this simplification, a system of equations can be created defining the evolution of concentration of unhealthy and healthy proteins.

$$\frac{\mathrm{d}p}{\mathrm{d}t} = \Delta \cdot (\mathrm{D} \cdot \Delta p) + k_0 - k_1 \cdot p - k_{12} \cdot p\,\tilde{p} \tag{4}$$

$$\frac{\mathrm{d}\tilde{p}}{\mathrm{d}t} = \Delta \cdot (\mathrm{D} \cdot \Delta \tilde{p}) - \tilde{k}_1 \cdot \tilde{p} + k_{12} \cdot p\,\tilde{p}. \tag{5}$$

This system is shown in equations (4) and (5) where D is the diffusion tensor defining the way the protein would spread through the network. When applying this system of equations to the Budapest connectome used within the original paper, the model remains largely the same. The only difference would be the replacement of the equation that defines the unhealthy protein concentration (See Equation 1) with the new system that defines both healthy and unhealthy protein concentrations. An identical diffusion tensor is used for both types of protein concentration. Therefore, how they move through the network are identical.

$$\frac{\mathrm{d}\tilde{p}}{\mathrm{d}t} = \Delta \cdot (\mathrm{D} \cdot \Delta \tilde{p}) + \left[k_{12}\frac{k_0}{k_1} - \tilde{k_1}\right]\tilde{p} - \frac{k_{12}^2 k_0}{k_1^2} \tag{6}$$

By making the assumption that initially $p \gg \tilde{p}$, we can estimate the value of p in terms of k_0, k_1 and k_{12}. Using a Taylor series, we can then substitute p into equation (4). This step creates equation (6), giving us the Fisher-Kolmogorov model as it provides an equation for a single misfolded protein concentration c. [1].

E. Protein concentration evolution

Damage to nodes was quantified using the variable $q_k \in [0, 1]$ (0 healthy, 1 maximal damage), modelled using the following equation:

$$\beta = 0.25 years^{-1} \qquad \gamma = 0.125 years^{-1}$$

$$\dot{q}_k = \beta c_k \left(1 - q_k\right), \quad q_k(0) = 0, \quad k = 1, \ldots, N, \tag{7}$$

$$\dot{w}_{kj} = -\gamma w_{kj} \left(q_k + q_j\right), \quad k, j = 1, \ldots, N. \tag{8}$$

1. *Seeding the graph*

The initial setup had $c_k(0) = 0$ for all nodes with the exception of the seed nodes. The seed nodes, $c_{26}(0)$ and $c_{68}(0)$ were both set at 0.025. These seed nodes were chosen due to their entorhinal location within the Budapest Connectome [6], being associated with the early stages of dementia as well as misfolded tau aggregation in AD.

2. Evolution of averaged toxic concentration and damage

Displaying the impact of different levels of damage on the average concentration of toxic proteins and damage in neural networks can deepen our understanding of the biophysical processes of neurodegenerative diseases, such as AD. By comparing the dynamic changes under different levels of damage, it is possible to observe how the disease affects the brain network over a long time scale, including the accumulation of toxic protein concentrations and network damage. This helps to understand how the disease progressively affects different areas of the brain and leads to the decline of cognitive functions.

To explore the evolutionary process, several key model equations are involved, including the temporal evolution of the toxic protein concentration equation (1), the temporal evolution of the node damage equation (7), and the temporal evolution of edge weights equation (8). c_k is the concentration of toxic proteins at node k, q_k is the degree of damage at node k, L_{k_j} are the elements of the graph Laplacian, α is the conversion rate and β is the toxicity coefficient. These are used in a differential equation model to simulate the evolution of the neural network over time.

F. Resting-state brain dynamics

In our investigation, we aimed to replicate the methodologies utilized by Goriely et al. [1] for analyzing the decline of cognitive functions via resting-state brain dynamics. These dynamics unfold on timescales that range from seconds for resting-state activity to years for the progression of the disease. Accordingly, the disease dynamics are considered quasi-stationary during the short observational windows. At time $t = T$, the connectome $\mathcal{G}_T$ is assumed to be constant despite its being ever-changing, allowing for the examination of resting-state activity.

Drawing on the foundational model presented by Goriely et al., we engaged a neural-mass model at each node, which simulates large-scale excitatory and inhibitory neural interactions akin to the Wilson-Cowan framework, as cited in their study [9, 16]. The intrinsic dynamics of the uncoupled nodes exhibit characteristics of a supercritical Hopf bifurcation, leading to an exponential decay of activity as the system approaches a stable fixed point. This behaviour is captured in figure (2), which displays the exponential decay of excitatory and inhibitory amplitudes for node 5 when it is uncoupled, oscillating around a frequency of approximately 40 Hz. The condition of each node k is described by a complex variable z_k, with the fundamental component reflecting excitatory population activity and the imaginary component corresponding to inhibitory population activity.

In our simulations of the network $\mathcal{G}_T$, weights $W = W(T)$ facilitate the interaction between neural populations via the excitatory component as in equation (10). The coupling term may allow the network of nodes to have sustained oscillation, as can be seen from the activity plots and the phase plots in figure (3). The interaction is further modulated by the sigmoidal function $S(x) = 1/(1 + e^{-x})$ through a delay differential equation.

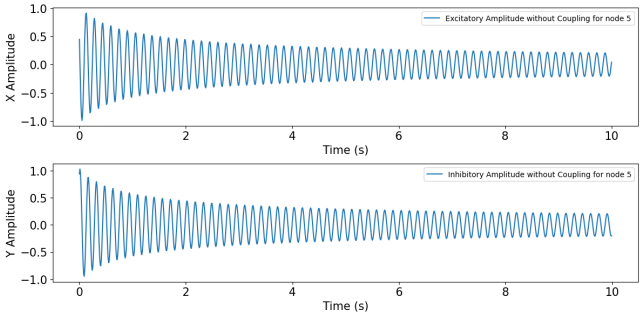

FIG. 2: Temporal evolution of excitatory (top panel) and inhibitory (bottom panel) amplitudes for node 5 in an uncoupled state, demonstrating an exponential decay with predominant oscillations at approximately 40 Hz. This reflects the decay dynamics characteristic of a supercritical Hopf bifurcation in a neural mass model.

$$\dot{z}_k = F(z_k) + \kappa S\left(\mathrm{Re}\left(\sum_{j=1}^{N} w_{kj} z_j\,(t-\tau_{kj})\right)\right) \tag{9}$$

$$\begin{aligned}\frac{\partial X_k}{\partial t} =& \lambda X_k - \omega_k Y_k - X_k(X_k^2+Y_k^2) \\ &+ kS\left(\sum_{j=1}^{N} w_{kj} x_j(t-\tau_{kj})\right)\end{aligned} \tag{10}$$

$$\frac{\partial Y_k}{\partial t} = \lambda Y_k + \omega_k X_k - Y_k(X_k^2+Y_k^2) \tag{11}$$

The internal dynamics of each node are described by $F(z_k) = z_k(\lambda + i\omega_k - |z_k|^2)$, with a decay rate $\lambda = -0.01$, intrinsic frequencies $\omega_k = \omega + \delta_k = 40$ Hz $+\delta_k$, where δ_k are randomly sampled from a normal distribution with zero mean and a variance of 0.1 Hz. The coupling gain $\kappa = 10$ and delays τ_{kj} are scaled according to node distances within the connectome data. These parameters are selected to mirror the neural-mass model, which aligns with fMRI observations during rest states [9].

1. Discretising the delays

In the resting-state brain dynamics simulations, an important consideration is the communication delay between different regions of the brain. These delays depend on the length of axonal fibres and the signal transmission speed, which was considered to be 1.5 m/s, as

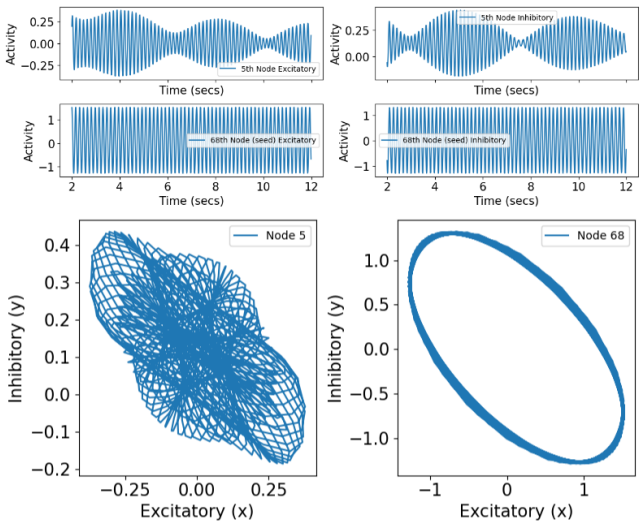

FIG. 3: Top panels display the excitatory (left) and inhibitory (right) neural activities for node 5 after introducing coupling to the system, illustrating the transition to sustained oscillations indicative of network interactivity. The bottom panels show the phase plots for nodes 5 (left) and 68 (right), with node 5 exhibiting complex oscillatory patterns, while node 68 demonstrates a limit cycle, providing insights into the diverse dynamical states achievable within the network. These behaviours emphasize the critical role of coupling in facilitating rich dynamical regimes across the brain's connectome.

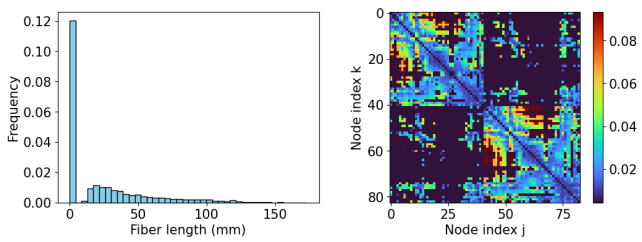

FIG. 4: Analysis of transmission delays in the brain's connectome. The top panel illustrates the probability density function of inter-nodal delays, providing an overview of prevalent transmission times within the network. The bottom panel presents a heatmap of these delays post-discretization into 40 distinct temporal categories, essential for modeling the dynamics of neural communication with a degree of computational efficiency.

referenced by Goriely et al. [1]. The delay distribution provides insight into the typical timeframes for neural signal propagation across the connectome, as evidenced in figure (4). To simplify the computational model without losing essential dynamics, these delays were discretized into 40 distinct categories. This discretization process allows for incorporating realistic transmission times into the coupling term as τ_{kj} while simulating the excitatory signal as in the equation (10). However, during the investigation of the resting state dynamics after each year of disease progression, the speed and the fiber length were kept constant.

With the original graph $\mathcal{G}_0$, collective oscillations are noticed, and in the absence of coupling, the amplitudes decline exponentially, displaying a frequency near 40 Hz.

G. Dynamic biomarkers

In our endeavour to replicate the decline in cognitive functions described in [1], we reimplemented three dynamic indices derived from a 10-second simulation of the resting state brain dynamics, encapsulated in the equation (9). These indices are:

(a) Overall power in the gamma range, expressed as:

$$P(T) = \int_{\Gamma} \mathrm{PSD}(\langle z \rangle)(\Omega)\, d\Omega, \tag{12}$$

where PSD is the power spectral density of $\langle z \rangle = \frac{1}{N}\sum_{j=1}^{N} \mathrm{Re}(z_j)$, and Γ denotes the Gamma frequency band.

(b) Average Oscillatory Activity, determined by:

$$A(T) = \frac{1}{N}\sum_{j=1}^{N} \frac{1}{t_{\mathrm{sim}}} \int_0^{t_{\mathrm{sim}}} |z_j(t)|\, dt, \tag{13}$$

representing the mean signal magnitude over all nodes throughout the simulation duration.

(c) Metastability Index, calculated as:

$$B(T) = \frac{1}{N}\sum_{j=1}^{N} \sigma_t^2(|z_j(t)|), \tag{14}$$

where σ_t^2 signifies the variance of the signal's magnitude within the simulation time frame.

For each regional set R_s, these measures P_s, A_s, and B_s are summed over their respective nodes and normalized accordingly. These biomarkers are known to be indicative of cognitive faculties and have links to neurodegenerative diseases [17].

H. Homeostasis

To replicate the original study's findings on neural network homeostasis, the dynamic nature of neuronal connections was taken into account. These connections are not static but rather adapt in response to ongoing neural dynamics, contributing to the maintenance

of network homeostasis [18]. We reimplemented a simple model of homeostatic adaptation, which maintained the average connectome coupling over time [1]. Given a homeostatic adaptation parameter $\xi \in [0, 1]$, the initial weight matrix is $W(0)$, and the scaled weight matrix at time T is updated according to:

$$\overline{\mathbf{W}}(T) = \left[(1-\xi) + \xi \left(\frac{\|\overline{\mathbf{W}}(T-1)\|}{\|\mathbf{W}(T)\|}\right)\right] \mathbf{W}(T) \quad (15)$$

for T = 1, 2, ... where $\|\cdot\|$ denotes the matrix norm. ξ the parameter that ranges between 0 and 1 scales the connectome weights annually, adjusting the network changes that accompany disease progression. At $\xi = 0$, the network undergoes no homeostatic changes, and alterations are exclusively due to the disease's impact. At $\xi = 1$, the network fully adapts, maintaining an invariant average coupling weight throughout the disease progression. This adaptation ensures that changes in coupling strength within one region due to the disease are balanced by compensatory changes in other regions, thus preserving the overall coupling strength of the network.

This approach facilitates reproduction of the original weighted connectome, essential for simulating resting-state dynamics that reflect the network's adaptation to neurodegenerative processes. The interplay between the evolving structural network and the associated cognitive functionalities could thus be scrutinized throughout the disease's progression.

III. RESULTS

A. Evolution of averaged toxic concentration and damage

By exploring the averaged toxic protein concentrations, node damage and edge weights in this system (seeing Fig. 5), it is possible to observe how node damage affects disease progression. The red line W can be interpreted as representing the extent of network destruction, with the dashed line indicating rapid network degradation within 15 years ($\beta = 4, \gamma = 2$), employing unrealistic parameters, while the solid line illustrates severe damage ($\beta = 1/4, \gamma = 1/8$). Over time, it is observable that the trajectories of protein concentration change in scenarios of severe damage closely align with those of undamaged networks ($\beta = 0, \gamma = 0$), suggesting negligible differences between them. By setting the damage parameters to unrealistic values for comparison with the severely damaged case, it becomes evident that network destruction does not significantly impact the increase in toxic protein concentration, indicating that network destruction does not markedly slow the progression of the disease but merely delays the onset to some extent [1].

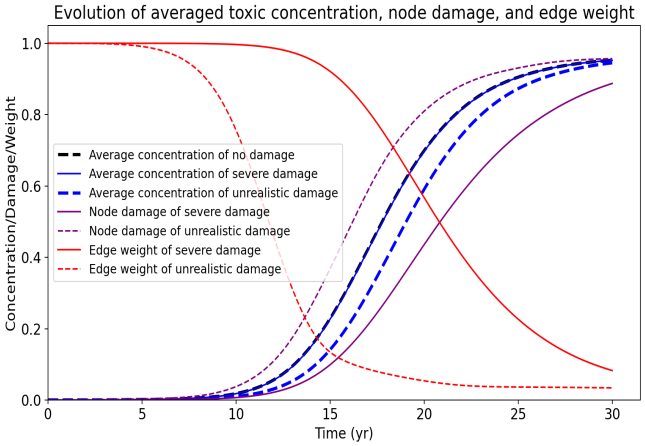

FIG. 5: The evolution of toxic protein concentration, node damage and edge weight over time with different degrees of damage.

B. Disease Progression

When recreating the model, The same trends in regional damage can be observed as that in the paper. The limbic region receives the most damage initially due to the entorhinal nodes becoming located in the limbic 'Super region'. This damage is then quickly seen in the temporal and parietal regions due to their nodes adjacency to the limbic region. However, the limbic region's damage increase is slower compared to the other regions. Likely due to the lower edge weights of the connections going to these nodes. (See Figure 6)

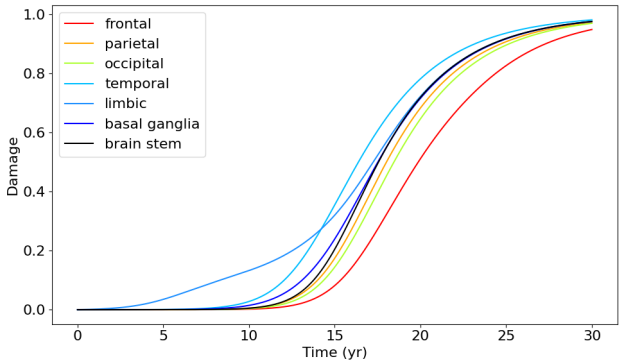

FIG. 6: This figure demonstrates the increase in damage over time using the original model found in the paper.

C. Heterodimer model

For further analysis, we also compared the results of the Fisher-Kolmogorov-Petrovsky-Piskunov model with that of a simple Heterodimer model. Those models displayed similar results except with a slower overall

growth rate of damage in all regions. The model also differed in how one region's damage affected the next. In the original model, the damage in each region started increasing in a similar time period, whereas when looking at the Heterodimer model, a slight difference in rate at which damage grows can be observed, this causes. Prior damage can be seen to have a greater effect on the rate at which future damage occurs, resulting in a 'flatter' graph in Figure (7).

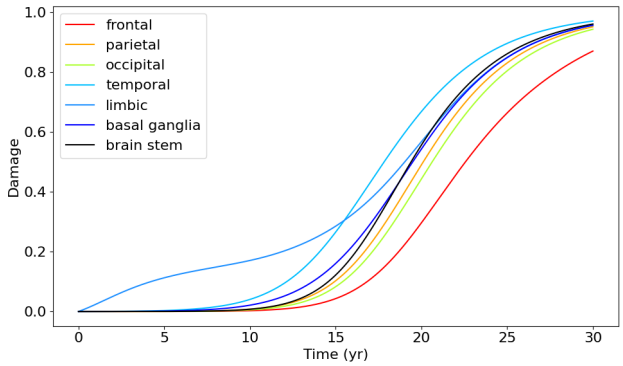

FIG. 7: The above figure shows the damage in each region using the Heterodimer model. The 'c' value in the original model is replaced with the $\widetilde{p}$ in the Heterodimer model.

D. Protein Seeding

Two key factors to consider when seeding misfolded proteins into the model are the location of the seeded nodes and the concentration of the proteins seeded. The first factor we explored was the concentration of the seeded protein. We compared the results of setting the seeded nodes to a protein concentration of 0.1 through to 1, this was compared against each other and then to the default concentration in the original model (0.025). As expected, a higher initial protein concentration caused the damage in the network to propagate faster than a lower one. The rate of damage growth remained consistent when comparing regions against one another, no matter the protein concentration. (See Figures 8 and 9)

E. Inter-hemisphere variation

Damage progression is varied across nodes (figure 10), with the variation in time of onset of damage, rates of change and final severity, with a variation seen within the connectome as a whole (A) as well as within single regions (B, C, D). Our results seem to indicate a generally higher and faster increase in damage in the left hemisphere nodes within a region. This divergence varied regionally however, in limbic nodes there is clear

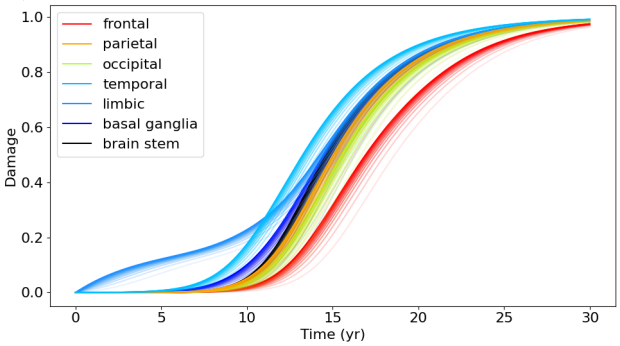

FIG. 8: This figure demonstrates the damage over time in the network on a per-region basis. The seed protein concentrated is also changed in this figure with more opaque colours having higher seed concentrations.

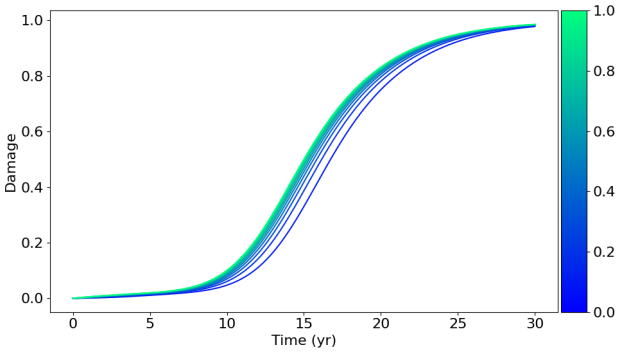

FIG. 9: This figure demonstrates the effect the seeded protein concentration has on the global damage growth within the network.

separation between left and right hemisphere nodes (figure 10 C), however in temporal and basal ganglia nodes (figure 10 B and D) there was far more overlap. The pattern of damage can vary considerably between different hemispheres, even within the same region and presumably equivalent nodes.

The difference in damage between pairs of equivalent nodes between hemispheres (figure 11) shows a fairly consistent pattern, with divergence rising to a peak, then lowering again as the damage approached the theoretical maximum of 1. In most cases, that damage generally accumulates faster in the left hemisphere than the right, though there are many nodes where the opposite is true.

F. Cognitive decline after physical damage

In the numerical implementation of dynamic biomarker calculations within neural networks, the code utilizes advanced signal processing techniques. The Gamma range power as in equation (12) is estimated

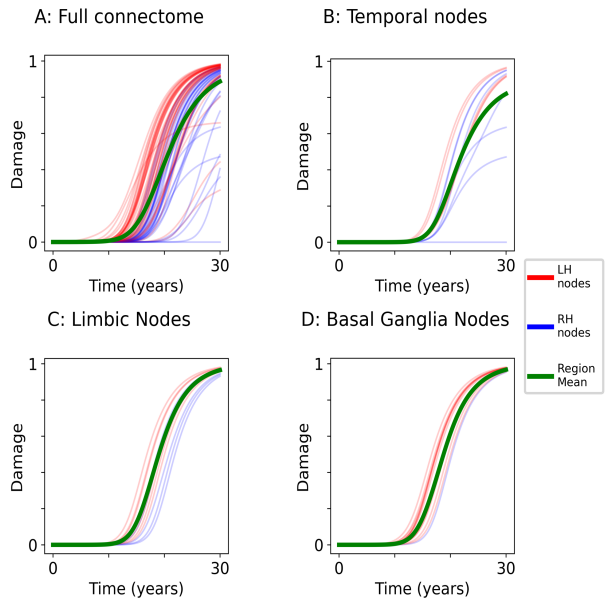

FIG. 10: Progression of damage within individual nodes in a variety of regions, coloured according to hemisphere. A: All nodes in the connectome. B: Nodes within the temporal region. C: Nodes within the limbic system. D: Nodes within the basal ganglia

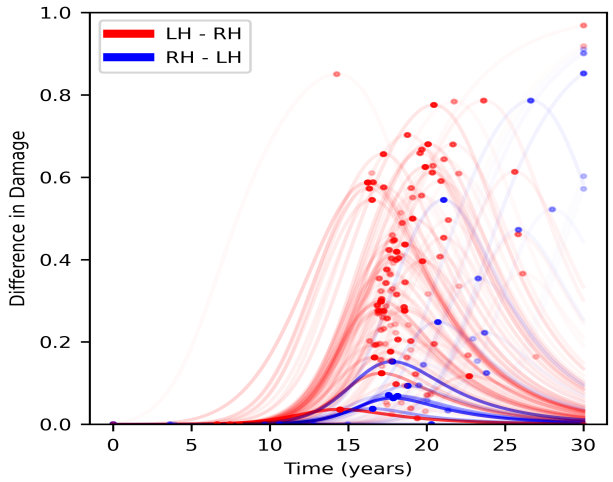

FIG. 11: Difference in damage between equivalent nodes across hemispheres: Red lines represent where damage is greater in the left hemisphere, whereas blue indicates the opposite. The peak divergence for each pair of nodes is indicated by the dots.

through the Welch method, an approach that segments the signal, applies windowing, and computes an averaged periodogram to derive the power spectral density (PSD). This PSD is then interpolated and integrated across a specified frequency band to calculate PT. For the average oscillatory activity as in equation (13), the trapezoidal rule integrates the absolute values of the neural activity signal over time. The metastability index as in equation (14) (BT) is computed as the mean variance of the signal magnitude, reflecting the temporal fluctuations in neural activity. Both global and regional metrics are extracted, providing a comprehensive analysis of network dynamics through these biomarkers, which are pivotal in understanding the functional connectivity and stability of the brain under various conditions.

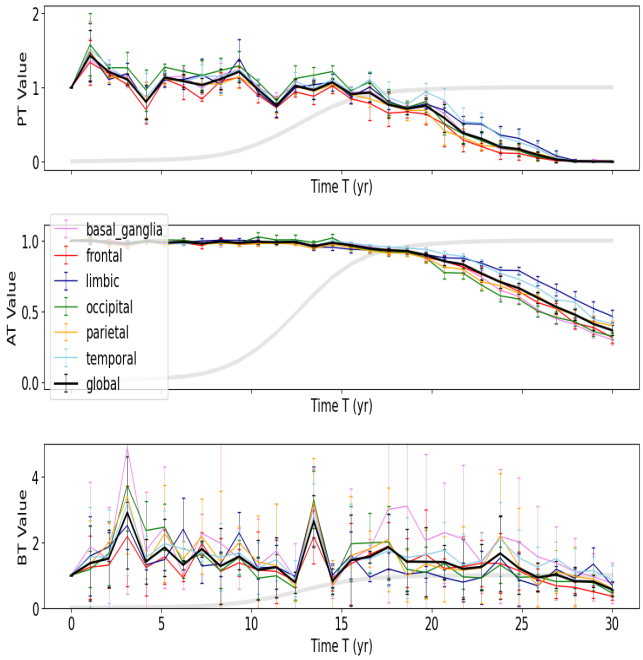

FIG. 12: Evolution of Dynamic Brain Biomarkers Over Time. This figure displays the mean and standard deviation of dynamic biomarkers, representing Gamma range power (PT), average oscillatory activity (AT), and metastability index (BT) across years for three different intrinsic frequency realizations. A stable profile is observed for up to 20 years, beyond which a marked decline correlates with physical damage in the brain. The early decline in oscillatory activity within the occipital lobe suggests its critical role in disease onset, which is different from the original findings [1].

The average amplitude provides an overview of neural activity levels, and the metastability index is interpreted as a proxy for information processing [19]. To assess the disease's influence on neural dynamics, we replicated the simulations on an evolving brain connectome at incremental time points T as in equation (9). The methodological details are accessible in the supplementary text of Goriely et al.'s work [1]. The figure (12) portrays the mean values and standard deviations of these dynamical markers, normalized against the baseline of a healthy brain at T=0 across 6 realizations. This visualization reveals a parallel trend to the original study, maintaining stability for up to 20 years into the disease's progres-

sion. Although the brain endures substantial structural damage by this juncture, as illustrated in our figure (5), the brain exhibits prolonged resilience to such structural damage.

However, beyond this period, there is an evident shift in dynamics, observable in the diminished capacity of nodes to sustain oscillatory activities, a phenomenon our reproduction accurately reflects with a more pronounced variability as noted in the lowest panel of the figure (12). Localized dynamical markers elucidate the disparity in how the disease's spread alters neural dynamics, with our data revealing a decrease in oscillatory activity within the occipital lobe that heralds the onset of global dynamic shifts. Unlike the original study, where the decline in the temporal lobe's oscillatory activity precedes global alterations, which may be because of the discrepancy in the structural connectivity matrix we worked with as in figure (1). These observations indicate that the rate of damage accumulation and network topology play critical roles in determining the threshold for oscillatory dynamics deterioration.

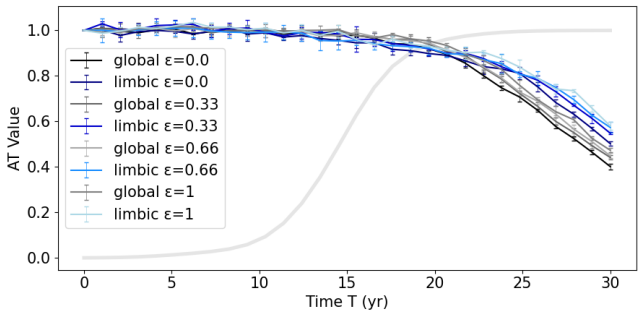

FIG. 13: Variations in oscillation amplitude correlate with changes in the homeostasis parameter based on 3 realizations. Increasing homeostatic modifies the progression of amplitude decline without affecting the initial timing of this decrease. The global mean oscillation amplitude (grey/black lines) shows how the slope varies for different homeostasis parameters; in the extreme case $\xi = 1$, the oscillation amplitude remains as in figure (12). In a similar pattern, the average amplitude observed in the limbic lobe, represented by blue lines, demonstrates consistent behaviour. For reference, C(T) is shown as the solid grey line.

G. Adaptation slows Cognitive Decline

In this study, the resting-state dynamics were replicated, as delineated by equation (9), with the inclusion of a homeostatic adjustment mechanism described in equation (15). The resultant data, illustrated in figure (13), delineate the evolution of the mean amplitude A(T) as the disease progresses across a spectrum of values for the adaptation parameter ξ. It was observed that increasing homeostatic control did not precipitate a change in the initial stage (around year 13), where oscillatory activity begins to decline. Instead, it appeared to mitigate the rate of neural degeneration. However, it was assumed that when cognitive functions begin to diminish past a specific threshold, such deceleration in disease progression could potentially also delay the commencement of the critical transition phase.

Additionally, figure (13) shows the mean oscillation amplitude within the limbic lobe. Notably, a decline in oscillatory activity globally preceded the limbic region, irrespective of the adaptation parameter's magnitude. This pattern persisted even with maximal adaptation ($\xi = 1$), wherein the aggregate oscillatory activity remained relatively unchanged within the observed timeframe of 30 years. This suggests a compensatory upregulation in other cerebral regions to maintain near-steady overall neural activity, which is consistent with the original work [1]. Hence, within the confines of this rudimentary model of adaptation, the fluctuation in oscillation amplitude may act as an early indicator of the overarching transition in the system's dynamics, regardless of the degree of homeostatic adaptation.

H. Decay in speed slows Global Cognitive Decline

Assuming that the speed is dependent on fibre connectivity between two nodes, our aim here was to capture the decay in speed within a neural network system. Assuming, that the speed is dependent on fiber connectivity between two nodes represented by a series of weight matrices across multiple time points. The method operates by computing the Euclidean norms of consecutive weight matrices similar to equation (15), thereby quantifying the magnitude of change in neural connectivity between time points. By comparing these norms, a decay rate is derived, reflecting the relative change in connectivity strength over time. This decay rate is then utilized to adjust the speed of transmission between the nodes, influencing the dynamics of the neural network model. Overall, the method offered no drastic shift in the decline of the average oscillatory amplitude for the global as well as the limbic region, as shown in figure (14).

IV. DISCUSSION

Decay in axonal velocity Our model assumes a constant axonal transmission speed (1.5 m/s), even as structural and functional degradation occurs. However, emerging research suggests that this speed may decline as diseases like Alzheimer's progress, influencing the delays calculated between nodes in our neural network model as in figure (4). Notably, the reduction of axonal velocity is a recognized consequence of Alzheimer's, elucidated in the recent study by [Author

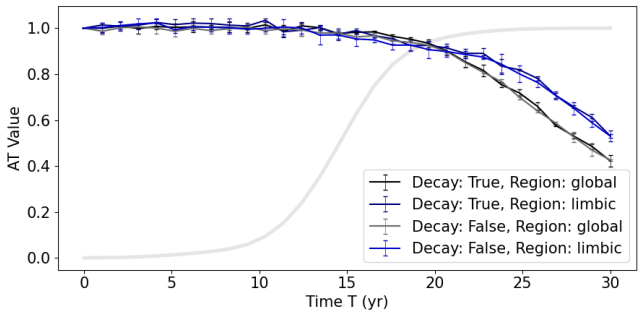

FIG. 14: Alterations in oscillation amplitude are observed with and without the decay in the speed based on 3 realizations. The mean oscillation amplitude (black/gray lines) globally and for region limbic (blue/light blue) does not vary much after including the decay in the speed when compared to speed being constant as in the original paper. For reference, C(T) is shown by the solid grey line.

et al., 2023], which provides a detailed account of how Alzheimer's affects axonal velocity and its underlying mechanisms [20]. Complementary findings from animal models also support this hypothesis, as observed in a murine Alzheimer's model, which showed a correlation between the presence of the disease and a diminished conduction speed [21]. Moreover, observations of decreased axonal velocity in peripheral human nerves further corroborate this assertion, as documented in the literature [22]. To incorporate these findings into our model, we propose modifying the constant axonal transmission speed to a variable that declines over time in correlation with disease progression. Such modification can be expressed through a set of equations governing the decay in transmission speed along with adaptation. Advancing on the results in figure 14, this integrated model can effectively capture the dynamic changes in neural communication as the disease advances. This refinement may provide a more accurate simulation of the brain's connectivity and could shed light on the timing and extent of cognitive decline. By incorporating a decaying speed factor into the delay calculations—effectively a function of both path length and a dynamically reducing velocity parameter—the model will provide a more nuanced depiction of neurodegenerative progression, potentially improving the prediction accuracy of cognitive impairment stages."

Hemispheric Differences Variation within a region was not surprising given the varied edges and weights of nodes. The rise then fall of damage asymmetry also makes sense given how we quantified damage, with equivalent nodes converging as theoretical maximum damage is approached due to the lagging hemisphere catching up. Distribution of peaks and damage progression show different patterns between the hemispheres generally and also within individual regions. This is interesting, as the seed nodes were the entorhinal nodes in both hemispheres. Asymmetric progression of Alzheimer's is well established with divergent rates of atrophy seen by Bugiani et al[23], with left leading progression more common, though there were cases of the opposite. This demonstrated that either hemisphere can lead in asymmetrical progression. Our results aligned, also showed a general trend of faster disease progression in the left hemisphere compared to the right, with exception a variety of exceptions. Tremblay et al[24] corroborated left hemisphere bias in cases with significant asymmetry, though most cases did present with significant asymmetry. However, this comparison covered the hemispheres as a whole and individual regions were often noted to be different. Results (10 show broad variation in damage within a single region and between equivalent nodes of opposite hemispheres (figure [**fig:hemisphere˙plot**]) it would be interesting to compare our findings for individual nodes to biological equivalents, for a more detailed analysis.

The budapest connectome [6] is constructed from an amalgamation of scans, so the distinct individual differences within people may have been lost. Given this limitation there may be some utility in running our model on data taken from single individuals. Tremblay et al[24] also found that divergence increases with progression, contradicting our results (figure 11). This may be due to the limitations of our model, which quantifies damage somewhat simplistically. Alternatively, it may be due to the fact that out model has a specified simulation time span of 30 years, in contrast, people may simply die when disease severity becomes great enough. If patients die before the lagging hemisphere catches up, this would lead to a pattern of increased divergence until death. We could extend the model by implementing a way to estimate time of death following disease onset, and see if the asymmetric difference in damage until time of death more closely models the progression in real patients.

Brain Connectome The results of our replication of Goriely et al.'s model align with those in the original paper [1]. However, the connectome used has great importance in modelling disease progression. Using a different connectome could cause different dynamics depending on the edge weights and node categorization used. Therefore, experimenting with other connectomes could help make the model more generalisable as it would highlight any discrepancies that occur due to the connectome data. Some such connectomes are the HCP Lifespan connectomes. Connectomes such as these could allows us the model the differences in disease progression between age groups [25]. Another key consideration is the directionality that is inherent in axonal bundles. This would cause asymmetry within the weight matrix and therefore greatly effect the dynamics occurring within neurodegenerative disease progression. However, no human brain connectomes currently exist that are suitable for used in this model. A directional mouse connectome exists that has been used for modelling protein transport but to truly understand human neurodegenerative diseases a human connectome would

be best [26].

Regional Network Damage and Protein Seeding An important factor to consider when looking at regional network damage are the location of the seed nodes. The entorhinal nodes were used as the seed nodes due to them exhibiting the earliest signs of damage from Alzheimer's disease [27]. Experimenting with other seed nodes may be valuable in providing information on the progression of damage and disease in other neurodegenerative disorders. This model is based upon that in Weickermen et al [14], who were able to model the prgression of other neurodegenerative diseased such as Parkinson's disease and amyotrophic lateral sclerosis (ALS) through modelling the spread of α-synuclein, and TDP-43, respectively.

Many neurogenerative diseases such as ALS act beyond the brain, causing deterioration of motor neurons within nerve cells and the spinal cord [28]. Given the success of [14] at modelling ALS within the brain, extending the model to also include nodes for the spinal cord or peripheral nerves, with the aim to better model ALS progression, could provide beneficial information on the progression of the disease.

Another possible scenario that could be explored would be the possibility of nodes in multiple regions being seed nodes, which would inevitably alter disease progression. It would allow us to model different diseases more appropriately. This could potentially prove more accurate when modelling a disease like Huntington's, which is unlikely to start in a single location due to its nature as a genetic disease and the ubiquity of the expression of the toxic protein Huntingtin. Despite these differences, Huntington's progression shows some evidence for prion-like mechanisms[29], and areas of high Huntingtin concentration have already been located within the striatum (specifically the caudate nucleus and putamen)[30] that show promise as seed nodes. Applying this information to the model would allow us to gain a better insight into how the regional damage changes as the disease progresses.

V. CONCLUSION

We were able to replicate the model and key findings for Goriely et al [1]. This included their findings that adge weight alteration over the course of disease progression had little impact on overall disease progression (figure 5). We were also able to replicate the disease staging they observed using their model (figure 6) as well as when implementing a heterodimer model of protein spread (figure 7). Fornari et al's[10] heterodimer model did not track limbic nodes, so by using the regions used in Goriely et al[1], we were able to show that limbic disease progression precedes all other regions in a heterodimer model too. Similarly to Goriely et al, we found a decline in neural biomarkers with disease progression (figure 12)

Investigating the difference in damage between hemispheres we were able to find variation in disease progression within nodes of a region and between regions (figure 10) broadly in line with biological findings. Differences between equivalent nodes in different hemispheres were observed, demonstrating the model is capable of capturing asymmetric progression (figure 11). Analysis of the dynamic biomarkers revealed their predictive capacity for a substantial decline in cognitive functions spanning a ten-year period.

Overall, the model created by Goriely et al[1] provided insights into the dynamics that occur within neurodegenerative diseases and how they affect brain function [1]. By experimenting with their model, we were able to both confirm their findings and obtain some novel insights, as well as potential avenues for further exploration.

VI. ACKNOWLEDGEMENTS AND CONTRIBUTIONS

Zongyuan Cai, Zakaria Taghi, Shayan Shafquat, and Youssef Hafid made equal contributions to all facets of this research. They collaborated in conceptualization, methodology design, data analysis, result interpretation, and manuscript preparation. Their collective effort ensured a comprehensive approach to advancing scholarly knowledge in the field. Many thanks to Dr. Markus Owen for is assistance and guidance with this project. We would also like to thank Alain Goriely, Ellen Kuhl and Christian Bick for creating the model, and their assistance with obtaining materials to replicate it.

REFERENCES

1. Goriely A, Kuhl E, and Bick C. Neuronal Oscillations on Evolving Networks: Dynamics, Damage, Degradation, Decline, Dementia, and Death. Phys. Rev. Lett. 2020 Sep; 125(12):128102
2. Jack CRJ, Bennett DA, Blennow K, Carrillo MC, Dunn B, Haeberlein SB, Holtzman DM, Jagust W, Jessen F, Karlawish J, Liu E, Molinuevo JL, Montine T, Phelps C, Rankin KP, Rowe CC, Scheltens P, Siemers E, Snyder HM, Sperling R, and Contributors. NIA-AA Research Framework: Toward a biological definition of Alzheimer's disease. Alzheimer's & Dementia 2018; 14(4):535–62
3. Scheltens P, Blennow K, Breteler MM, De Strooper B, Frisoni GB, Gauthier S, Jones LA, et al. Alzheimer's disease. The Lancet 2021; 397(10284):1577–90
4. Thangwaritorn S, Lee C, Metchikoff E, Razdan V, Ghafary S, Rivera D, Pinto A, and Pemminati S. A Review of Recent Advances in the Management of Alzheimer's Disease. Cureus 2024 Apr
5. Jucker M and Walker LC. Self-propagation of pathogenic protein aggregates in neurodegenerative diseases. Nature 2013 Sep; 501:45–51

6. Szalkai B, Kerepesi C, Varga B, and Grolmusz V. Parameterizable consensus connectomes from the Human Connectome Project: the Budapest Reference Connectome Server v3.0. Cognitive Neurodynamics 2016 Sep; 11:113–6
7. Calignon A de, Polydoro M, Suárez-Calvet M, William C, Adamowicz DH, Kopeikina KJ, Pitstick R, Sahara N, Ashe KH, Carlson GA, Spires-Jones TL, and Hyman BT. Propagation of Tau Pathology in a Model of Early Alzheimer's Disease. Neuron 2012 Feb; 73:685–97
8. Wilson HR and Cowan JD. A mathematical theory of the functional dynamics of cortical and thalamic nervous tissue. Kybernetik 1973 Sep; 13:55–80
9. Deco G, Jirsa V, McIntosh AR, Sporns O, and Kötter R. Key role of coupling, delay, and noise in resting brain fluctuations. Proceedings of the National Academy of Sciences 2009 Jun; 106:10302–7
10. Fornari S, Schäfer A, Jucker M, Goriely A, and Kuhl E. Prion-like spreading of Alzheimer's disease within the brain's connectome. Journal of The Royal Society Interface 2019 Oct; 16:20190356
11. Henderson MX, Cornblath E, Darwich A, Zhang B, Brown H, Gathagan RJ, Sandler RM, Bassett DS, Trojanowski JQ, and Lee VMY. Quantitative α-synuclein pathology mapping and network analysis provide a framework for understanding pathological protein spread. Nature Neuroscience 2019; 22:1248–57
12. McNab JA, Edlow BL, Witzel T, Huang SY, Bhat H, Heberlein K, Feiweier T, Liu K, Keil B, Cohen-Adad J, Tisdall MD, Folkerth RD, Kinney HC, and Wald LL. The Human Connectome Project and beyond: Initial applications of 300mT/m gradients. NeuroImage 2013; 80:234–45
13. Raj A, Kuceyeski A, and Weiner M. A Network Diffusion Model of Disease Progression in Dementia. Neuron 2012 Mar; 73:1204–15
14. Weickenmeier J, Jucker M, Goriely A, and Kuhl E. A physics-based model explains the prion-like features of neurodegeneration in Alzheimer's disease, Parkinson's disease, and amyotrophic lateral sclerosis. Journal of the Mechanics and Physics of Solids 2019 Mar; 124:264–81
15. Prusiner SB, Scott M, Foster D, Pan KM, Groth D, Mirenda C, Torchia M, Yang SL, Serban D, Carlson GA, Hoppe PC, Westaway D, and DeArmond SJ. Transgenetic studies implicate interactions between homologous PrP isoforms in scrapie prion replication. Cell 1990 Nov; 63(4):673–86
16. Deco G, Cabral J, Woolrich MW, Stevner A, Van Hartevelt TJ, and Kringelbach ML. Single or multiple frequency generators in on-going brain activity: A mechanistic whole-brain model of empirical MEG data. NeuroImage 2017; 152:538–50
17. Uhlhaas PJ and Singer W. Neural synchrony in brain disorders: relevance for cognitive dysfunctions and pathophysiology. Neuron 2006; 52:155–68
18. Markram H, Gerstner W, and Sjöström PJ. Spike-Timing-Dependent Plasticity: A Comprehensive Overview. Frontiers in synaptic neuroscience 2012 Jan; 4
19. Rabinovich MI, Afraimovich V, Bick C, and Varona P. Information flow dynamics in the brain. Physics of life reviews 2012 Mar; 9:51–73
20. Dan L and Zhang Z. Alzheimer's disease: an axonal injury disease? Frontiers in Aging Neuroscience 2023 Oct; 15
21. Gelman S, Palma J, and Ghavami A. Axonal Conduction Velocity in CA1 Area of Hippocampus is Reduced in Mouse Models of Alzheimer's Disease. Journal of Alzheimer's Disease 2020 Oct; 77:1383–8
22. Qian X, Yue L, Mellor D, Robbins NM, Li W, and Xiao S. Reduced Peripheral Nerve Conduction Velocity is Associated with Alzheimer's Disease: A Cross-Sectional Study from China. Neuropsychiatric Disease and Treatment 2022 Feb; Volume 18:231–42
23. O, Bugiani J, Constantinidis B, Ghetti C, Boura F, and Tagliavini. Asymmetrical cerebral atrophy in Alzheimer's disease. Clinical neuropathology 1991 Feb; 10:55–0
24. Tremblay C, Serrano GE, Intorcia AJ, Curry J, Sue LI, Nelson CM, Walker JE, Glass MJ, Arce RA, Fleisher AS, Pontecorvo MJ, Atri A, Montine TJ, Chen K, and Beach TG. Hemispheric Asymmetry and Atypical Lobar Progression of Alzheimer-Type Tauopathy. Journal of Neuropathology amp; Experimental Neurology 2022 Feb; 81:158–71
25. Bookheimer SY, Salat DH, Terpstra M, Ances BM, Barch DM, Buckner RL, Burgess GC, Curtiss SW, Diaz-Santos M, Elam JS, Fischl B, Greve DN, Hagy HA, Harms MP, Hatch OM, Hedden T, Hodge C, Japardi KC, Kuhn TP, Ly TK, Smith SM, Somerville LH, Uğurbil K, Kouwe A van der, Essen DV, Woods RP, and Yacoub E. The Lifespan Human Connectome Project in Aging: An overview. NeuroImage 2019 Jan; 185:335–48
26. Oh SW, Harris JA, Ng L, Winslow B, Cain N, Mihalas S, Wang Q, Lau C, Kuan L, Henry AM, Mortrud MT, Ouellette B, Nguyen TN, Sorensen SA, Slaughterbeck CR, Wakeman W, Li Y, Feng D, Ho A, Nicholas E, Hirokawa KE, Bohn P, Joines KM, Peng H, Hawrylycz MJ, Phillips JW, Hohmann JG, Wohnoutka P, Gerfen CR, Koch C, Bernard A, Dang C, Jones AR, and Zeng H. A mesoscale connectome of the mouse brain. Nature 2014 Apr; 508:207–14
27. Igarashi KM. Entorhinal cortex dysfunction in Alzheimer's disease. Trends in Neurosciences 2023 Feb; 46(2):124–36
28. Morris J. Amyotrophic Lateral Sclerosis (ALS) and Related Motor Neuron Diseases: An Overview. The Neurodiagnostic Journal 2015 Sep; 55(3):180–94
29. Donnelly KM, Coleman CM, Fuller ML, Reed VL, Smerina D, Tomlinson DS, and Pearce MMP. Hunting for the cause: Evidence for prion-like mechanisms in Huntington's disease. Frontiers in Neuroscience 2022 Aug; 16
30. Monte SM de la, Vonsattel JP, and Richardson EP. Morphometric Demonstration of Atrophic Changes in the Cerebral Cortex, White Matter, and Neostriatum in Huntington's Disease. Journal of Neuropathology Experimental Neurology 1988 Sep; 47(5):516–25